nature physics
SUPPLEMENTARY INFORMATION
DOI: 10.1038/NPHYS3715

Coincidence of a high-fluence blazar outburst with a PeV-energy neutrino event

1 Supplementary Methods

VLBI Imaging: The TANAMI VLBI images of PKS B1424−418 (Fig. 1) are based on observations on 2011 Nov 13, 2012 Sep 16, and 2013 Mar 14 with the Long Baseline Array (LBA) and associated telescopes in Australia, New Zealand, South Africa, Chile, and Antarctica. Correlation of the data was performed with the DiFX correlator[46] at Curtin University in Perth, Western Australia. The data were calibrated and imaged following Ojha et al. (2010)[17]. Supplementary Table 1 gives an overview of the array configuration and image parameters. The noise level for each image was determined by fitting a Gaussian function to an off-source part of the image. For this purpose and for producing the final images shown here we used the software package ISIS 1.6.2[47].

The TANAMI array varies in configuration for each observation, leading to inhomogeneous sampling of the visibility data. This results in a different noise level and restoring beam in the final images. In order to compare the images, they were created with the maximum noise level of all three images (1.1 mJy/beam) and the enclosing beam for convolution, i.e. the restoring beam which encompasses the synthesis beam of all observations (here $2.26 \times 0.79\,\mathrm{mas}^2$ at a position angle of $9.5°$). In addition, Fig. 1 shows the individual images restored with the individual beams and contours starting at $3\sigma_{\mathrm{RMS}}$. The brightness temperature T_{B} and size of the central emission region diameter d_{core} from each observation were determined by fitting a two-dimensional Gaussian function to the visibility data. T_B was then calculated following standard procedures[48]. By adopting a cosmology[49] with $H_0 = 73\,\mathrm{km\,s^{-1}\,Mpc^{-1}}$, $\Omega_\Lambda = 0.73$ and $\Omega_m = 0.27$ for the conversion from angular to linear scales, $1\,\mathrm{mas}$ corresponds to about $8.3\,\mathrm{pc}$ at a redshift of $z = 1.522$.

***Fermi*/LAT γ-ray data analysis:** For the analysis of *Fermi*/LAT γ-ray data, we used the *Fermi* Science Tools (v9r32p5) with the reprocessed Pass 7 data and the P7REP_SOURCE_V15 instrument response functions[50] and a region of interest (ROI) of 10° in the energy range 100 MeV to 300 GeV. We applied a zenith angle limit of 100° and the GTMKTIME cut DATA_QUAL==1 && LAT_CONFIG==1 && ABS(ROCK_ANGLE)<52. We used the Galactic diffuse emission model GLL_IEM_V05.FITS and the isotropic diffuse model ISO_SOURCE_V05.TXT. The model consists of all 2FGL sources inside the ROI. For the spectral and light-curve analysis, the normalization constants of all model sources were left free. The source spectral index was left free for the spectral analysis and frozen for the light curve analysis during the modeling of the spectrum. The γ-ray light curve of PKS B1424−418 (Fig. 1) has been calculated using 14 day bins. We applied a Bayesian-blocks analysis[51] to the light curve. We used the change points to determine the onset of the outburst as 2012 Jul 16, which is marked as a shaded blue region in Fig. 1.

All γ-ray sources detected by *Fermi*/LAT with flares that exceeded the pre-defined threshold of $10^{-6}\mathrm{cm}^{-2}\,\mathrm{s}^{-1}$ ($>100\,\mathrm{MeV}$) are included in the *LAT Monitored Source List*. Light curves of all these sources are publicly available at `http://fermi.gsfc.nasa.gov/ssc/data/access/lat/msl_lc/`. By definition, this sample represents the brightest *Fermi*/LAT sources. We used this list to identify the sources with the highest γ-ray fluences and analyzed their γ-ray light curves in detail as described above. We integrated the light curves from 2012 Jul 16 through 2013 Apr 30 to determine the highest-fluence sources during the months around the arrival time of the 2 PeV IceCube neutrino event. PKS B1424−418 is the brightest blazar in terms of γ-ray fluence: $F = (30.5 \pm 0.3)\,\mathrm{cm}^{-2}$ (the uncertainty is statistical only). The next on the list are the blazars CTA 102 ($F = (20.0 \pm 0.3)\,\mathrm{cm}^{-2}$), and B2 1633+38 ($F = (18.2 \pm 0.3)\,\mathrm{cm}^{-2}$), which are both in the northern hemisphere.

Broadband SEDs: The broadband SED of PKS B1424−418 (Fig. 2) has been built from quasi-simultaneous data from *Fermi*/LAT, *Swift*/XRT, *Swift*/UVOT, SMARTS[52], ALMA, ATCA and the LBA. Archival data from 2MASS[53] and WISE[54] catalogs are included as well.

Swift/XRT data were reduced with standard methods, using the most recent software packages (HEASOFT 6.15.1) and calibration databases. Spectra were grouped to a minimum signal-to-noise ratio of 5. Spectral fitting was performed with ISIS 1.6.2[47]. We fitted the (0.5–10) keV energy band with an absorbed power law model, which yielded good results for all time ranges. The source showed no evidence of intrinsic X-ray absorption in excess of the Galactic value[55]. X-ray data were deabsorbed using the best available abundances[56] and cross-sections[57]. *Swift*/UVOT data were extracted following standard methods. Optical, infrared, and ultraviolet data were dereddened using the same absorbing columns[58]. At hard X-ray energies, we used data from *Swift*/BAT and *INTEGRAL*/IBIS from the energy bands of 20 keV to 100 keV and 20 keV to 200 keV, respectively. The source was not included in the BAT 70-month catalog[59], which was based on data between 2004 Dec and 2010 Dec. Using stacked BAT maps from the 104-month survey (2004

Dec through 2013 Aug), we detected the source and calculated the flux by applying a power-law fit to the spectrum. For *INTEGRAL*/IBIS we extracted a 2.5 σ upper limit from the variance of a mosaic combining all pointed observations in the time-range from 2011 Dec to 2013 Sep, where the source was located within 14 ° from the pointing direction. The 104-month average BAT flux value is in good agreement with the 2LAC SED, whose data time period overlaps (2008 Aug to 2010 Aug). It is marginally consistent with the SEDs corresponding to the post-2010 short-flare and the HESE period and well below the SED for the high-fluence period between 2012 Jul and 2013 Apr.

The broadband spectra were fit with two logarithmic parabolas[60] in order to parametrize the characteristic double humped structure. The spectral-model fit is performed in detector space while the fluxes in each energy bin in the top panel of Fig. 2 are calculated independent of the model[61], under the assumption of constant flux in each bin. Note that for curved spectra and wide energy bins, this approach can lead to an apparent positive offset of the flux data points over the best-fit model as seen, e.g., in the *Fermi*/LAT data points of the ‘short flare’ in Fig. 2. X-ray absorption and optical extinction were included in the broadband fit. Upper limits are generally not considered in the fits. The low γ-ray upper limits at the highest *Fermi*/LAT energies indicate a possible cutoff. Including the upper limits as values in the SED fits forces the parabolas to increase in peak flux in order to still describe the slope at X-ray energies and reduces the overall fit quality. The increase in peak flux leads to a higher neutrino estimate (see below), with the exception of the short flare, so that our method to ignore upper limits in the fit is more conservative for our purposes.

Neutrino event prediction: To derive maximal-possible neutrino events to be expected from the measured SEDs, we applied the techniques that we developed for our analysis of the AGN in the fields of the first two PeV IceCube events. We used 2FGL GeV γ-ray spectra[62] and extracted X-ray spectra taken during the same period by *Swift*[63]. For sources not observed by *Swift*, we used X-ray data or upper limits from the *ROSAT* all-sky survey[64]. For PKS B1424−418, we calculated in addition *Fermi*/LAT γ-ray spectra for the various time ranges of interest according to the methods described above. We fit a single log parabola to the high-energy data. From the integrated 1 keV to 5 GeV SEDs, we can derive a maximal-possible neutrino flux for each source. From this, we can derive the maximal-possible number of counts for the 988-day HESE livetime (see Table 3) using the appropriate effective area for northern/southern-hemisphere sources for electron neutrinos of the IceCube 988-day analysis[3]. Formal uncertainties of neutrino counts can be derived from the uncertainties of the integrated electromagnetic energy output but are dominated by systematic uncertainties due to the simplicity of the model and method. In particular, note that the overall shape of the SED changes during long time ranges and that the derived neutrino output from averaged LAT spectra is not necessarily equal to the sum of neutrino output from additive segments of the full time range, especially in the presence of a strong outburst. This systematic uncertainty is illustrated by the fact the maximal-possible neutrino output derived from the average 3-yr SED of PKS B1424−418 is 4.5 events, while the separate consideration of the 27-month pre-outburst phase and the 9-month outburst yields a higher maximal-possible neutrino output of 5.7 events (cf. Table 2).

Calculation of chance coincidences of major blazar outbursts and PeV neutrino events: We estimate the number of chance coincidences of major blazar outbursts and PeV neutrino events *a posteriori* using $N_{\rm coinc} = \dot{N}_\nu \times \dot{N}_{\rm outburst} \times \tau \times T$. Here, $\dot{N}_\nu$ is the number of PeV-neutrinos per year in the southern sky, $\Omega_{\rm south} = 2\pi$, $\dot{N}_{\rm outburst}$ is the number of major outbursts per year within a cone covered by the typical median uncertainty of shower-like PeV neutrino events of $\Omega_\nu \sim 0.16\,{\rm sr}$ (averaged median angular uncertainty of the three observed PeV events $\sim 13°$), τ is the coincidence time window defined by the outburst time, and T is the IceCube observation time of $T = 3\,{\rm yr}$, during which IceCube has observed three PeV events. We therefore obtain for $\dot{N}_\nu \sim 1\,{\rm yr}^{-1}$. High-fluence blazar outbursts occur on time scales of months so we choose, conservatively, $\tau = 1\,{\rm yr}$ for the time window for chance coincidences. In the *Fermi*/LAT blazar light curves for six years and for the whole sky, we find a total of eight 1 yr periods, during which an individual blazar reached or exceeded the GeV fluence of the PKS B1424−418 outburst. These high-fluence phases occured in the sources PKS B1424−418, PKS B 1222+216, 3C 273, 3C 454.3 (2 periods), and PKS B1510−089 (3 periods). Hence, the rate of such outbursts occurring within Ω_ν is expected to be $\dot{N}_{\rm outburst} \sim 0.1\,{\rm yr}^{-1}\,{\rm sr}^{-1} \times \Omega_\nu = 0.016\,{\rm yr}^{-1}$. Using these numbers, we end up with $N_{\rm coinc} \sim 0.05$ as the mean number of chance coincidences. The Poisson probability to observe one or more such coincidences is about 5%. However, because of the lack of a pre-defined statistical test, we cannot formally use this value to test the hypothesis of a chance coincidence.

2 Supplementary discussions

Coincidences of sub-PeV neutrino events with high-fluence blazars: All high-fluence blazars from Table 3 are in coincidence with more than one IceCube sub-PeV neutrino event, which is not surprising given the high probability of chance coincidences within the large R_{50} radii of the cascade-like IceCube events. In addition, up to 25 of the 34 sub-PeV events are of possible atmospheric-neutrino or cosmic-ray muon origin[3]. The two most interesting cases involve HESE-7, which coincides with long-lasting outbursts of the two high-fluence blazars PKS B0537−441 and PKS B2326−502. Both sources are located within the $\Omega^{R_{50}}_{\text{HESE-7}}$ field. The integrated fluence of PKS B0537−441 and PKS B2326−502 predicts a maximum of ~ 5 neutrino events, i.e., applying the scaling factor of 0.025, the Poisson probability for the detection of more than zero PeV events is about 12 %. The IceCube events HESE-16 and HESE-25 are close ($1.9R_{50}$ and $1.2R_{50}$, respectively) to the position of the top-ranked high-fluence source, PKS B1510−089. It is remarkable that the two observed events occurred close to the highest peaks of the GeV light curve but we emphasize again that a considerable fraction of IceCube events at these comparatively low energies can be of atmospheric origin and that the field of HESE-25 is particularly large.

Coincidences of track neutrino events with γ-ray blazars: We note that the IceCube track events, which have a much better angular resolution than the shower events, are all of rather low energy and/or are located at far northern declinations. Most of them are thus likely of atmospheric origin. In fact, event HESE-28 showed associated hits in the IceTop surface air shower array[2,3]. The IceCube team considers three additional track events particularly ambiguous, which started near the detector boundary and were down going (HESE-3, HESE-8, HESE-18, HESE-23). The positions of the remaining three (HESE-5, HESE-13, and HESE-37) which can be considered the most-likely track events to be of true extraterrestrial origin, have been compared with positions of known γ-ray AGN. One of these events (HESE-5) is spatially coincident with the blazar PKS 0723$-$008, but as pointed out previously[65], the chance probability for a *Fermi*/LAT detected AGN to coincide with any given field of about 1 deg^2 is high. We estimate the Poisson probability for HESE-5 from the known 1017 γ-ray AGN in the 2LAC catalog[24] distributed over the full sky (excluding the $|b| < 10^\circ$ region around the Galactic plane) to be 41 %. However, as mentioned already above, only half of all IceCube events are expected to hold the coordinates of their true astrophysical sources inside their R_{50} regions, while the other half are located at larger positional offsets. In this small sample of three track events, we thus expect only one or two coincidences within R_{50}. If we consider radii twice as large, we find one 2LAC blazar for HESE-13 (4C +41.11 at $1.8R_{50}$) and one for HESE-37 (RBS 0958 at $1.6R_{50}$). The *a posteriori* chance probability for all three track events to coincide within $2R_{50}$ with a 2LAC blazar is 22 %. None of the candidate blazars is of particularly high fluence. It is likely that they represent the large population of 'typical' 2LAC γ-ray blazars, which have low individual detection probabilities. However, their integrated emission plus the contribution of fainter unresolved blazars to the EGB is high and may lead to the detected events.

3 Supplementary References

46. Deller, A. T. et al., DiFX-2: A More Flexible, Efficient, Robust, and Powerful Software Correlator. *PASP*, **123**, 275-287 (2011)

47. Houck, J. C. & Denicola, L. A., ISIS: An Interactive Spectral Interpretation System for High Resolution X-Ray Spectroscopy. *Astronomical Data Analysis Software and Systems IX*, **216**, 591-594 (2000)

48. Kovalev, Y. Y., Kellermann, K. I., Lister, M. L., et al. Sub-Milliarcsecond Imaging of Quasars and Active Galactic Nuclei. IV. Fine-Scale Structure. *AJ*, **130**, 2473-2505 (2005)

49. Spergel, D. N., Bean, R., Doré, O., et al. Three-Year Wilkinson Microwave Anisotropy Probe (WMAP) Observations: Implications for Cosmology. *ApJS*, **170**, 377-408 (2007)

50. Ackermann, M., Ajello, M., Albert, A., et al. The Fermi Large Area Telescope on Orbit: Event Classification, Instrument Response Functions, and Calibration. *ApJ*, **203**, 4 (2012)

51. Scargle, J. D., Norris, J. P., Jackson, B., & Chiang, J. Studies in Astronomical Time Series Analysis. VI. Bayesian Block Representations. *ApJ*, **764**, 167 (2013)

52. Bonning, E., Urry, C. M., Bailyn, C., et al. SMARTS Optical and Infrared Monitoring of 12 Gamma-Ray Bright Blazars. *ApJ*, **756**, 13 (2012)

53. Skrutskie, M. F., Cutri, R. M., Stiening, R., et al. The Two Micron All Sky Survey (2MASS). *AJ*, **131**, 1163-1183 (2006)

54. Wright, E. L., Eisenhardt, P. R. M., Mainzer, A. K., et al., The Wide-field Infrared Survey Explorer (WISE): Mission Description and Initial On-orbit Performance. *AJ*, **140**, 1868-1881 (2010)

55. Kalberla, P. M. W., Burton, W. B., Hartmann, D., et al., The Leiden/Argentine/Bonn (LAB) Survey of Galactic HI. Final data release of the combined LDS and IAR surveys with improved stray-radiation corrections. *A&A*, **440**, 775-782 (2005)

56. Wilms, J., Allen, A., & McCray, R. On the Absorption of X-Rays in the Interstellar Medium. *ApJ*, **542**, 914-942 (2000)

57. Verner, D. A., Ferland, G. J., Korista, K. T., & Yakovlev, D. G. Atomic Data for Astrophysics. II. New Analytic FITS for Photoionization Cross Sections of Atoms and Ions. *ApJ*, **465**, 487-498 (1996)

58. Nowak, M. A., Neilsen, J., Markoff, S. B., et al., Chandra/HETGS Observations of the Brightest Flare Seen from Sgr A*. *ApJ*, **759**, 95 (2012)

59. Baumgartner, W. H., Tueller, J., Markwardt, C. B., et al., The 70 Month Swift-BAT All-sky Hard X-Ray Survey. *ApJS*, **207**, 19 (2013)

60. Massaro, E., Perri, M., Giommi, P., & Nesci, R. Log-parabolic spectra and particle acceleration in the BL Lac object Mkn 421: Spectral analysis of the complete BeppoSAX wide band X-ray data set. *A&A*, **413**, 489-503 (2004)

61. Nowak, M., Wilms, J., Heinz, et al. Is the 'IR Coincidence' Just That?, *ApJ*, **626**, 1006-1014 (2005)

62. Nolan, P. L., Abdo, A. A., Ackermann, M., et al. Fermi Large Area Telescope Second Source Catalog. *ApJS*, **199**, 31 (2012)

63. Gehrels, N. et al. The Swift Gamma-Ray Burst Mission. *ApJ*, **611**, 1005-1020 (2004)

64. Voges, W. et al. The ROSAT all-sky survey bright source catalogue. *A&A*, **349**, 389-405 (1999)

65. Brown, A. M., Adams, J., & Chadwick, P. M. γ-ray observations of extraterrestrial neutrino track event positions. *MNRAS*, **451**, 323-331 (2015)

4 Supplementary Tables

Supplementary Table 1: **Details of TANAMI VLBI observations of PKS B1424$-$418 and image parameters**

Date [yyyy-mm-dd]	$S_{\rm total}$ [Jy]	$S_{\rm peak}$ [Jy/beam]	$\sigma_{\rm RMS}$ [mJy/beam]	$b_{\rm maj}$ [mas]	$b_{\rm min}$ [mas]	P.A. [°]	$T_{\rm B,core}$ [10^{11} K]	$d_{\rm core}$ [pc]
2011 Nov 13	2.33 ± 0.23	1.80 ± 0.18	0.2	1.95	0.50	3.8	4.2	2.5
2012 Sep 16	3.17 ± 0.32	2.89 ± 0.29	0.4	2.20	0.71	4.0	7.4	2.2
2013 Mar 14	6.23 ± 0.62	5.61 ± 0.56	1.1	2.26	0.79	9.5	13	2.3

Note: Tabulated image parameters refer to the formal values after hybrid imaging using natural weighting[17]. The three images shown in Fig. 1 are all convolved with the same restoring beam and use uniform contour lines and color scaling. See Fig. 1 for the individual images restored with the individual beams and contours starting at $3\sigma_{\rm RMS}$. Core FWHM diameters $d_{\rm core}$ and $T_{\rm B,core}$ have been derived from fitting an elliptical Gaussian component to the visibility data.

Array configurations: PK-AT-HO-CD-TC-TD-HH-MP-WW (2011 Nov 13); PK-AT-HO-CD-TC-HH-AK-KE (2012 Sep 16); PK-AT-HO-CD-TC-TI-HH-WW-AK-KE (2013 Mar 14); PK: Parkes (64 m), AT: ATCA (5x22 m), HO: Hobart (26 m), CD: Ceduna (30 m), TC: TIGO (6 m), TI: Tidbinbilla (70 m), TD: Tidbinbilla (34 m), MP: Mopra (22 m), HH: Hartebeesthoek (26 m), WW: Warkworth (12 m), AK: ASKAP (12 m), KE: Katherine (12 m).

5 Supplementary Figures

Figure 1 **Supplementary Figure 1** – Individual TANAMI VLBI images of the core region of PKS B1424$-$418. Each image corresponds to the properties in Supplementary Table 1 for the individual observations. All contours start at $3\sigma_{\mathrm{RMS}}$ and increase logarithmically by factors of 2 .

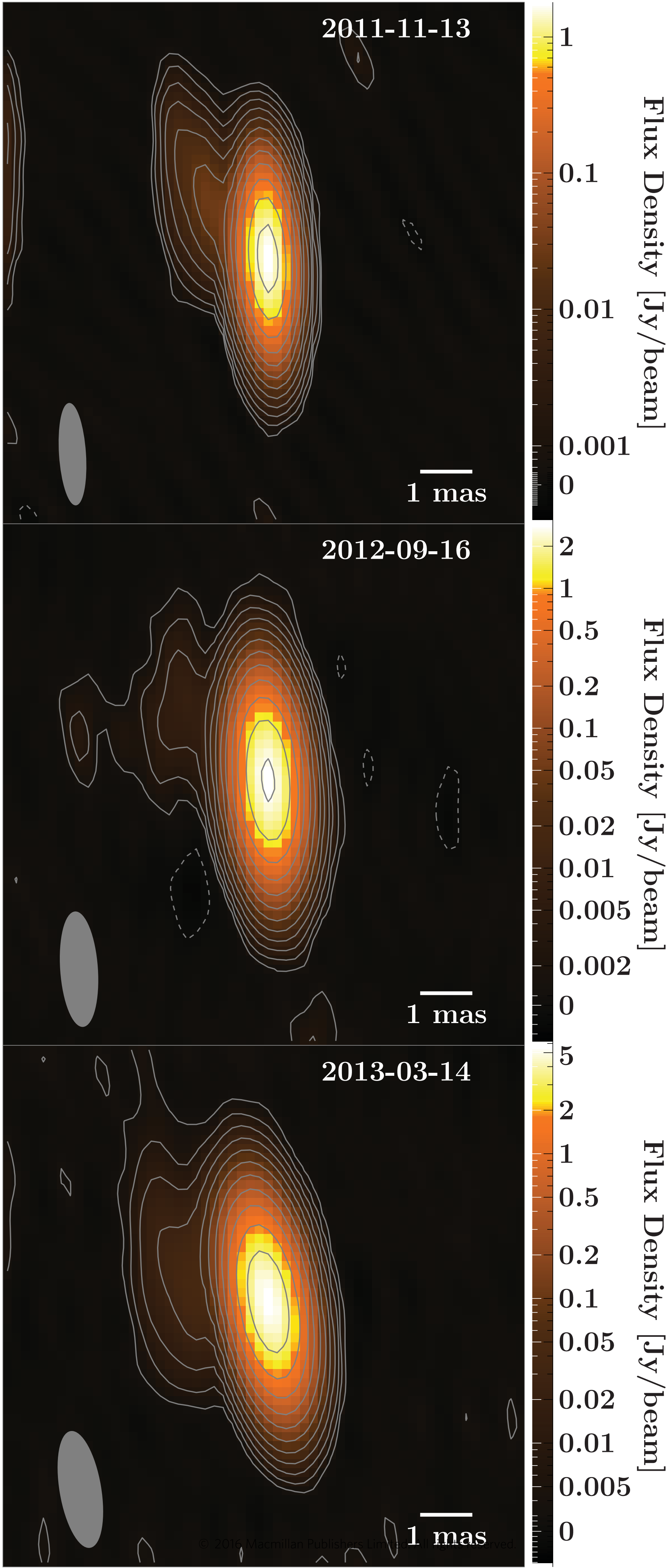
2011-11-13
1 mas
1
0.1
0.01
0.001
0
Flux Density [Jy/beam]
2012-09-16
1 mas
2
1
0.5
0.2
0.1
0.05
0.02
0.01
0.005
0.002
0
Flux Density [Jy/beam]
2013-03-14
1 mas
5
2
1
0.5
0.2
0.1
0.05
0.02
0.01
0.005
0
Flux Density [Jy/beam]